

Spatially Resolved Magnetic Resonance

Methods, Materials, Medicine, Biology,
Rheology, Geology, Ecology, Hardware

Edited by P. Blümmler, B. Blümich,
R. Botto, E. Fukushima

 **WILEY-VCH**

Weinheim · New York · Chichester
Brisbane · Singapore · Toronto

This Page Intentionally Left Blank

Spatially Resolved Magnetic Resonance

Edited by
P. Blümler, B. Blümich
R. Botto, E. Fukushima

 **WILEY-VCH**

This Page Intentionally Left Blank

Spatially Resolved Magnetic Resonance

Methods, Materials, Medicine, Biology,
Rheology, Geology, Ecology, Hardware

Edited by P. Blümmler, B. Blümich,
R. Botto, E. Fukushima

 **WILEY-VCH**

Weinheim · New York · Chichester
Brisbane · Singapore · Toronto

Editors:

Dr. Peter Blümler
Prof. Dr. Bernhard Blümich
Lehrstuhl für Makromolekulare
Chemie und Magnetic Resonance
Center, MARC, RWTH Aachen
Worringer Weg 1
D-52074 Aachen, Germany

Prof. Dr. Robert E. Botto
Chemistry Division
Argonne National Laboratory
9700 South Cass Avenue
Argonne, Illinois 60439-4828
USA

Dr. Eiichi Fukushima
2425 Ridgecrest Dr. SE
Albuquerque
New Mexico 87108
USA

This book was carefully produced. Nevertheless, authors, editors and publisher do not warrant the information contained therein to be free of errors. Readers are advised to keep in mind that statements, data, illustrations, procedural details or other items may inadvertently be inaccurate.

Cover picture: Velocity NMR image of shear bands in a cone-plate rheometer.
For details see chapter 49. Reproduced with permission of M. M. Britton
and P. T. Callaghan.

Library of Congress Card No. applied for
A catalogue record for this book is available from the British Library

Die Deutsche Bibliothek – CIP-Einheitsaufnahme

Spatially resolved magnetic resonance : methods, materials, medicine, biology, rheology, geology, ecology, hardware / ed. by Peter Blümler ... Weinheim ; New York ; Chichester ; Brisbane ; Singapore ; Toronto : Wiley-VCH, 1998
ISBN 3-527-29637-9

© WILEY-VCH Verlag GmbH, D-69469 Weinheim (Federal Republic of Germany), 1998

Printed on acid-free and low chlorine paper

All rights reserved (including those of translation into other languages). No part of this book may be reproduced in any form – by photoprinting, microfilm, or any other means – nor transmitted or translated into machine language without written permission from the publishers. Registered names, trademarks, etc. used in this book, even when not specifically marked as such, are not to be considered unprotected by law.

Printing: betz-druck GmbH, D-64291 Darmstadt
Bookbinding: Großbuchbinderei J. Schäffer, D-67269 Grünstadt
Printed in the Federal Republic of Germany

Foreword

Just as the „Heidelberg Conference“ has moved about, even as far as the American Southwest, it has broadened its scope to include essentially all non-clinical magnetic resonance imaging. The immense variety of techniques and applications in human diagnostic NMR imaging is driven by medical needs, but limited by considerations of safety, time, and economics. In the broader worlds of science and technology, the seemingly-unlimited ways spin magnetization can be manipulated, and the forms of matter that can be studied, are much more various, and the experiments involve a broader range of the knowledge and skills of physicists, chemists, and materials scientists. The addition of spatial resolution to the tools available for such studies allows them to be applied to many heterogeneous objects, and to processes, such as transport, that involve spatial dimensions on the supramolecular scale.

Still, however, much of the ingenuity of practitioners in the field is devoted to overcoming difficulties and artifacts that limit its usefulness. NMR, with or without imaging, is a powerful but fragile technique, and all too often promising approaches to beautiful experiments are blocked by ugly details. One way to read this volume is to look for the implicit terrain maps of practicality. What is being attempted, and why not something else? Why is a particular set of techniques, a particular piece of equipment, being used? Because it is available, or because nothing else will do? In clinical studies, the questions to be asked and the priorities are often better defined, but in other areas NMR spectroscopy and imaging often seem to be answers looking for questions. As practitioners learn more about the wider world, and outsiders become more familiar with the possibilities, limitations and peculiarities of magnetic resonance methods, the field is maturing. This volume documents a long stride toward such maturation and integration, along with the ever increasing power and subtlety of techniques and analyses, and should inspire developers and users in all areas, from medicine to geology.

Urbana, January 1998

Paul C. Lauterbur

Preface

In the year 1991 the First Conference on Magnetic Resonance Microscopy has taken place in Heidelberg, Germany. Based on the contributions to this meeting the book *Magnetic Resonance Microscopy: Methods and Applications in Materials Science, Agriculture and Biomedicine*, VCH Weinheim, 1992, had been edited by Bernhard Blümich and Winfried Kuhn and provided an up-to-date reference on the subject of non-medical imaging. At the time the methods in magnetic resonance imaging evolved largely from the area of clinical diagnostics, but were adapted more and more to other applications, and extensive studies on test phantoms demonstrated potential use in various fields of science and engineering.

Six years later, the *Fourth International Conference on Magnetic Resonance Microscopy* was held in Albuquerque, New Mexico, and it was felt, that an update of the Microscopy Book was needed. During this time, the field has advanced significantly, and several new techniques were introduced as well as interesting new applications covering such diverse areas as polymer and elastomer characterization, analysis of construction materials and material flow, various topics in biomedicine, and plants studies. The focus on microscopy features was broadened to include magnetic resonance of macroscopic systems. Applications in the area of oil-well analysis, and non-destructive quality and process control are made possible by the development of dedicated instrumentation which can readily be moved to the site of interest.

The editors are indebted to the authors for timely submission of their contributions and to the referees, who helped to improve a number of manuscripts. We are indebted to Tanja Rente for transforming the manuscripts into book format and to VCH for their cooperation and help with the final editing and production process.

September 1998

Peter Blümmler, Bernhard Blümich,
Robert E. Botto, and Eiichi Fukushima

Contents

Foreword

P. C. Lauterbur V

Preface

P. Blümler, B. Blümich, R. E. Botto, and E. Fukushima..... VI

Methods

1. Spatial Resolution in Spectroscopic Imaging

M. von Kienlin and R. Pohmann..... 3

2. CYCLOCROP Mapping of ^{13}C Labelled Compounds:
Perspectives in Polymer Science and Plant Physiology

*M. Heidenreich, A. Spyros, W. Köckenberger, N. Chandrakumar,
R. Bowtell, R. Kimmich*..... 21

3. Contrast Enhancement Based on Intermolecular Zero Quantum
Coherences for Magnetic Resonance Imaging and Microscopy

R. R. Rizi, S. Ahn, J. Hopkins, J. S. Leigh, and W. S. Warren 53

4. Frequency Dependence of EPR Sensitivity

G. R. Eaton, S. S. Eaton, and G. A. Rinard 65

5. SPRITE Imaging of Short Relaxation Time Nuclei

B. J. Balcom..... 75

6. Refocusing a Spin-Echo in the Presence of a Strong Readout
Gradient Field Using an Underdriven Gradient Pulse

G. Planinšič and M. Symms..... 87

7. The Analysis and Development of Pulse Sequences for
Self-Diffusion Weighted Stray-Field Imaging

A. J. Bohris, D. A. Faux, D. G. Gillies, and P. J. McDonald 95

8. Imaging Diffusion with Non-Uniform B_1 Gradients
K. Woelk, B. L. J. Zwank, J. Bargon, R. J. Klingler
R. E. Gerald II, and J. W. Rathke 103
9. In Situ Imaging of Charge Carriers in an Electrochemical Cell
R. E. Gerald II, R. J. Klingler, J. W. Rathke, G. Sandí, and K. Woelk..... 111
10. Efficient Simulation of Spin Echo, Gradient Echo, Fast, and
 Ultrafast NMR Imaging Sequences by Isochromat Summation
P. Shkarin and R. G. S. Spencer 121
11. A Novel Algorithm for Tumor Characterization by Analysis
 of Transversal Relaxation Rate Distributions in MRI
R. Martin and M. Martín-Landrove 133

Materials

12. Materials Imaging with Examples from Solid Rocket Propellants
W. E. Maas, L.H. Merwin, and D.G. Cory 141
13. ^{129}Xe MRM Characterization of Pore Structures in Silica Aerogels
D. M. Gregory, R. E. Gerald II, D. J. Clifford, and R. E. Botto..... 163
14. NMR Imaging of Mechanically Treated Polymers
B. Traub, S. Hafner, D. Maring, and H. W. Spiess..... 179
15. Soft-Matter Relaxation by the NMR-MOUSE
A. Guthausen, G. Zimmer, R. Eymael, U. Schmitz,
P. Blümmler, and B. Blümich 195
16. Application of NMR-Imaging to Industrial Polymers
M. Knörngen, U. Heuert, H. Schneider 211
17. Electron Spin Resonance Imaging (ESPRI) of Transport Processes
 in Polymeric Systems
S. Schlick, P. Eagle, K. Kruczala, and J. Pilar 221

18. Stray-Field Imaging and Magnetic Resonance Microimaging Studies of High Impact Polystyrene, an Elastomer-Toughened Material
J. A. Chudek, G. Hunter, F. Mohd Som, P. J. McDonald, and B. Newling 235
19. Mixed Solvent Ingress into PMMA Measured by Stray-Field Magnetic Resonance Imaging
D. M. Lane, P. J. McDonald, and J. L. Keddie 241
20. Stray-Field Imaging and Magnetic Resonance Microimaging Studies of the Anisotropic Absorption of Solvents by Extruded Polypropylene
R. J. Abbott, J. A. Chudek, G. Hunter, R. L. MacKay, P. J. McDonald, and L. Squires 253
21. NMR Microimaging: A Useful Tool to Study the Dissolution of Solids
N. Black, T. Vienneau, and Y. Pan 259
22. Observation of the Water Distribution During Drying of Textiles
J. Leisen, L. Hou, H. W. Beckham, and W. W. Carr 265
23. A Broad-Line Magnetic Resonance Imaging Study of Water Transport in Cementitious Building Materials
A. J. Bohris, U. Goerke, P. J. McDonald, M Mulheron, B. Newling, and B. Le Page 273
24. Stray-Field Imaging and Magnetic Resonance Microimaging Studies of Water Intrusion/Stress Mobilisation in Dense Polymer Systems Used in Construction
S. N. Scrimgeour, G. Hunter, W. J. Harvey, C. H. Lloyd, D. M. Lane, and P. J. McDonald 281
25. Stray-Field Magnetic Resonance Imaging of Hardening Materials
T. G. Nunes, P. R. Bodart, and E. W. Randall 287
26. Applications of Stray-Field Imaging to Dental Materials Science
S. N. Scrimgeour, C. H. Lloyd, G. Hunter, D. M. Lane, and P. J. McDonald 293

27. Particle Compaction as Observed by MRI
*R. A. Waggoner, M. Nakagwa, S. J. Glass, M. Reece,
 and E. Fukushima*..... 299

Medicine and Biology

28. ^2H Double Quantum Filtered NMR Histology and Diffusion
 Measurements in Isolated Nerves and Blood Vessels
H. Shinar, Y. Sharf, U. Eliav, Y. Seo, and G. Navon..... 307
29. Translational Diffusion of Water in Lung Tissue
B. Geil, D. C. Ailion, G. Laicher, and A. G. Cuttillo..... 323
30. Studies of Perfused Brain Slices with MR Microscopy
J. D. Bui, D. L. Buckley, M. I. Phillips, and S. J. Blackband..... 337
31. Application of NMR Micro-Imaging to the Study of Water Transport
 in Eye Lenses
B. A. Moffat, R. J. W. Truscott, M. H. J. Sweeney, and J. M. Pope..... 345
32. Relaxation Anisotropy as a Possible Marker for
 Macromolecular Orientations in Articular Cartilage
Y. Xia 351
33. Morphometric Analysis of Cartilage Grown in a Hollow Fiber
 Bioreactor Using NMR Microscopy
K. Potter, K. W. Fishbein, W. E. Horton, and R. G. S. Spencer 363
34. EPR Imaging of the Rat Heart
J. L. Zweier and P. Kuppusamy..... 373
35. Application of High Resolution Cardiac Magnetic Resonance
 Imaging to Monitor a Rodent Model of Cardiac Dysfunction
*S. Chandra, K. G. Gurbanov, R. Strittmatter, E. H. Ohlstein,
 G. Z. Feuerstein, and S. K. Sarkar* 389
36. Fast MR Imaging of Esophageal Motility
*Y. Seki, S. Naruse, Y. Seo, M. Murakami, T. Ozaki, M. Kitagawa,
 H. Ishiguro, Y. Nakae, and T. Hayakawa*..... 395

37. Spatial NMR Studies of Tumor Spheroids
K. R. Minard, R. A. Wind, W. E. Maas, K. Millis, and D. G. Cory 403
38. ^{19}F Chemical Shift Imaging of F-nuc Formed from 5-FU in
 Mouse Tumor by Fast Spin Echo
Y. Doi and Y. Kanazawa 413
39. ^{17}O and ^{31}P Magnetic Resonance Imaging and Spectroscopy:
 In Vivo Investigations of Cell Bioenergetics
G. D. Mateescu, M. Cabrera, and D. Fercu 421
40. Volume Localized ^1H MRS of Renal Osmolytes
G. J. Cowin, I. A. Leditschke, S. Crozier, and Z. H. Endre 431
41. MRM in the Modeling of the Ossicular Chain
*E. W. Abel, J. A. Chudek, G. Hunter, R. M. Lord,
 R. L. MacKay, and R. P. Mills* 439
42. NMR Imaging of Rigid Biological Tissues
*Y. Seo, H. Takamiya, H. Ishikawa, T. Nakashima,
 Y. Sharf, and G. Navon* 445
43. Magnetic Resonance Microimaging of Teeth
*S. N. Scrimgeour, C. H. Lloyd, G. Hunter,
 J. A. Chudek, and R. L. MacKay* 459
44. MRM, an Alternative Approach to the Study of Host/Parasitoid
 Relationships in Insects
*J. A. Chudek, G. Hunter, R. L. MacKay, S. Moritz, A. N. E. Birch,
 I. E. Geoghegan, R. J. McNicol, and M. E. N. Majerus* 467
45. Plant Growth Studies Using Low Field NMR
*L. van der Weerd, T. Ruttink, D. van Dusschoten,
 P. J. Vergeldt, P. A. de Jager, and H. Van As* 473
46. Fast Spatially Resolved Displacement Imaging in (Bio)Systems
T. W. J. Scheenen, D. van Dusschoten, P. A. de Jager, and H. Van As ... 481

Diffusion and Flow

47. Generalized Treatment of Modulated Gradient Spin Echo Attenuation for Restricted Diffusion in Spherical Pores
S. L. Codd and P. T. Callaghan..... 489

48. NMR-Imaging Techniques for Quantitative Characterization of Periodic Motions: 'Incoherent Averaging' and 'Spectral Side Band Analysis'
U. Goerke and R. Kimmich..... 499

49. Shear-Banding in a Cone-and-Plate Rheometer
M. M. Britton and P. T. Callaghan..... 507

50. Applications of NMR Flow Imaging in Material Science
S. Laukemper-Ostendorf, K. Rombach, and P. Blümler..... 517

51. A Non-Invasive Investigation of Concentration Polarization in Crossflow Microfiltration of Colloidal Silica
D. Airey, V. Chen, J. Wu, and J. M. Pope 531

52. Evaluation of Mixing Profiles of Power Law Fluids in Scraped Surface Heat Exchanger Geometry Using MRI
W. Wang, J. H. Walton, M. J. McCarthy, and K. L. McCarthy..... 539

53. The Self Diffusion of 1,3 Propylene Glycol in Track Etched Membrane Pores
E. Vasina, V. Skirda, V. Volkov, A. Nechaev, and B. Mchedlishvili..... 547

Geology and Ecology

54. Review: NMR Detection and Characterization of Hydrocarbons in Subsurface Earth Formations
R. L. Kleinberg, and C. Flaum 555

55. Why Would an Oil Company Use MRI?
B. A. Baldwin and R. L. King..... 575

56. Pore Structure and Connectivity of Porous Rock by High Resolution NMR Microscopy
D. A. Doughty and L. Tomutsa 603

57. Relaxation-Diffusion Processes and Local Magnetic Field Distributions in Natural Porous Media
D. Pérez, A. Benavides, S. González, D. Barrantes, and M. Martín-Landrove 617

58. MR Microscopy of Savannah River Tank Waste Simulants
K. R. Minard, R. A. Wind, and L. O. Dworjany..... 627

Hardware

59. A Compact, Superconducting Magnet for Magnetic Resonance Microscopy
S. Crozier and D. M. Doddrell 639

60. MRI Gradient Coil Optimization
F. D. Doty 647

61. Novel, Asymmetric Gradient Coil Sets for Magnetic Resonance Microscopy
S. Crozier, W. U. Roffmann, and D. M. Doddrell..... 675

62. Novel Gradient Coils for Magnetic Resonance Microscopy
E. R. Andrew, M. Kempka, S. Sagnowski, and E. Szczesniak..... 683

63. The NMR Endoscope
R. Haken, P. Blümmler, and B. Blümich 695

64. Development of a Flexible Pulse Programmer for MRI Using a Commercial Digital Signal Processor Board
K. Kose and T. Haishi..... 703

Tutorial

65. Introduction to Magnetic Resonance	
<i>Y. Xia</i>	713
Author Index	741
Subject Index	745

Methods

This Page Intentionally Left Blank

1. Spatial Resolution in Spectroscopic Imaging

Markus von Kienlin and Rolf Pohmann

Physikalisches Institut (Biophysik) Universität Würzburg, D-97074 Würzburg, Germany

Abstract

This contribution reviews various aspects of the spatial resolution obtained in spectroscopic imaging experiments. After showing the fundamental difficulty to define “spatial resolution”, it is shown that the precision in the determination of the location of a point source is only limited by the signal-to-noise ratio, and is much better than the nominal resolution. Then the resolving power is analyzed using the Rayleigh criterion, and the importance of a sufficient digital resolution is illustrated. Finally, the importance of the “spatial response function” is emphasized.

1.1 Introduction: Localized Spectroscopy

Most conventional methods to examine physiologic parameters or metabolic processes directly in living tissue require to extract a sample, which then is analyzed with biochemical means. These biopsies in animals or humans can not only be painful, but often carry some risk. *Localized NMR spectroscopy* provides non-invasive biopsy: it can analyze the chemical composition of well defined regions within the body, without the need to extract a specimen. Localized NMR spectroscopy therefore has not only found many applications in fundamental research, where it contributes to a better understanding of metabolism, but is also gaining importance in clinical diagnostics. To these ends, a high quality and reliability of localization is prerequisite, and huge research efforts have been made to improve the sensitivity, the spatial resolution, the stability and the patient comfort of these techniques.

First attempts to acquire NMR spectra within a larger object employed surface coils [1,2] or shaped the homogeneous region of the main, static magnetic field (“topical magnetic resonance TMR” [3–5]). P. Bendel *et al.* were the first to acquire spectroscopic information in the presence of a magnetic field gradient [6]. The first to employ pulsed magnetic field gradients and selective excitation pulses to select a voxel within the sample were W. Aue *et al.* [7]. Their work started the development of a large number of techniques which allow to measure the spectrum of more or less rectangular volumes; the best known of these are DRESS [8], ISIS [9], STEAM [10–12] and PRESS [13]. These single voxel techniques today tend to be replaced by “spectroscopic imaging”, also called “chemical shift imaging CSI [14,15].” CSI has become available to a large number of users through the advent of actively shielded gradient systems and more sophisticated instruments. It offers the advantage to measure spectra not only in a single volume element, but simultaneously in a whole grid of many volumes across the sample, thus allowing to compare local variations within the studied object.

In this contribution, we analyze the spatial resolution obtained in spectroscopic imaging. The knowledge of the spatial resolution is important for further technical developments, but it is also crucial for the correct interpretation of spectroscopic images. After a more precise definition of the topic, the basic principle of Fourier imaging will be briefly introduced. The concept of the spatial response function will be described, followed by an in depth analysis of the spatial resolution. Finally, the impact of numerical data representation will be clarified.

1.2 What is “Spatial Resolution”?

The goal of localized NMR spectroscopy *in vivo* is to acquire spectra from well circumscribed anatomical areas. To achieve high specificity, a good discrimination from neighboring regions is essential, the contamination by signals from other regions must be as low as possible. It is furthermore advantageous to have as small a sensitive volume as possible, which fits well into the target region, and to avoid as much as possible tissue heterogeneity. The major hurdle is the poor sensitivity of NMR spectroscopy, which usually imposes the lower limit for the size of the sensitive volume.

While this qualitative description of the goal of *spatial resolution* is straightforward, it is much more difficult to define a quantitative measure for the spatial resolution. The notion “spatial resolution” can be interpreted in many different ways. A possible meaning can be the precision, by which the location of a signal source within the sample can be determined. Another and completely different definition is to measure the minimal distance between *two* signal sources within the sample, which still allows to distinguish them. Both definitions allow to calculate some specific number for the spatial resolution of some measurement method. Such a number does allow to compare various methods – its significance is nevertheless questionable. In biomedical applications, there are no point sources of NMR signal, but one has to deal with extended and heterogeneous regions with irregular shape. The knowledge of the “*spatial response function SRF*” is essential for a correct interpretation of the results, and to estimate the degree of possible signal contamination from adjacent regions. The *SRF* indicates the weight of the contribution of every point in space to a localized spectrum. The shape of the *SRF* essentially depends on the number of image points, the sampling scheme, and eventual filtering and other parameters of the acquisition and the sample. It is therefore not sufficient to indicate only the nominal resolution of the experiment: one should also show the *SRF*! Other circumstances which can further deteriorate the quality of localization – like motion artifacts or diffusion – will not be considered in the following.

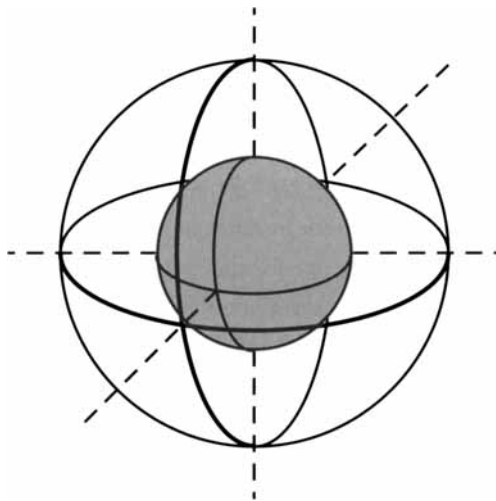


Fig. 1.1: The spatial resolution is mainly limited by the low sensitivity. If a spectrum with sufficient SNR can be acquired from the large sphere in only 10 min, it takes almost 11 hours (!) to obtain a spectrum with the same SNR from the smaller sphere with half the diameter!

The issue of spatial resolution is mainly due to the low *sensitivity* of NMR spectroscopy. As demonstrated in Fig. (1.1), the low sensitivity is the main obstacle to increase the spatial resolution. The detected NMR signal is directly proportional to the sample magnetization within the sensitive volume. If the spin distribution is homogeneous, the signal decreases with the third power of the linear dimension of the volume. The signal-to-noise ratio (SNR) is proportional to the square root of the total duration of an experiment, the duration required to achieve some given SNR therefore depends to the sixth power of the linear dimension of the sensitive volume.

At the current state of coil and receiver technology, where the SNR already is mainly dominated by the properties of the sample, substantial further improvements in sensitivity cannot be expected. Sensitivity thus sets a lower limit to the size of volumes selected in localized spectroscopy. If their *size* can hardly be reduced, it is nevertheless possible to improve their *sharpness*. The following sections show which parameters influence the shape of the *SRF*, and how that shape can be improved in spectroscopic imaging.

1.3 Fourier Methods for Spectroscopic Imaging

The most common way to acquire spectroscopic images is based on a *Fourier method* proposed by A. Kumar *et al.* [14]. As early as 1979, A. Maudsley applied phase encoding and Fourier reconstruction to map an inhomogeneous magnetic field by measuring the spatial dependence of the resonance frequency [16]. Successful experiments both on phantoms [15,17] and *in vivo* [18,19] have shown the numerous advantages of spectroscopic imaging, which now is being used in an increasing number of clinical studies. A more detailed survey can be found for instance in [20].

The simplest possible pulse sequence for spectroscopic imaging is plotted in Fig. 1.2. The excitation pulse is followed by a short gradient pulse of length τ_G in one, two or all three directions, which encodes the spatial information as phase modulation of the transverse magnetization. Then, all gradient fields are switched off and the signal of the freely precessing spins is detected. This experiment is repeated for some number of repetitions, applying regularly incremented gradient strengths. The spectroscopic image is then obtained by applying Fourier-transformations in all spatial and the spectral dimensions. This simple sequence can be modified by generating spin-echoes or stimulated echoes, or by using slice-selective excitation or refocusing pulses, but these variations do not affect

the basic principle of spectroscopic imaging. In the following mathematical description only one spatial dimension is treated, the generalization to two or three dimensions is straightforward.

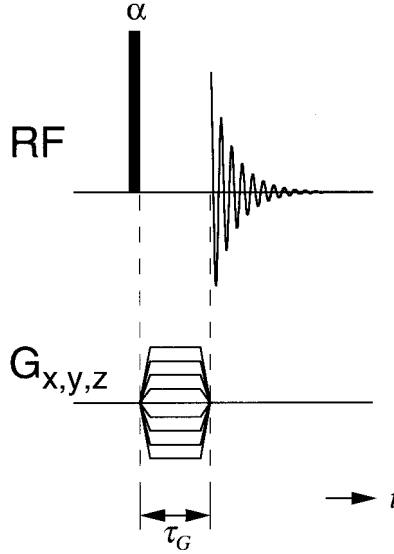


Fig. 1.2: A pulse sequence of spectroscopic imaging. After excitation, gradients are switched on for a short time to modulate the phase of the magnetization. The signal is then acquired in the homogeneous field.

The volume covered by the spectroscopic image is usually called “field-of-view” (*FOV*). The nominal resolution Δr_{nom} is the size of the image elements (voxels). For an image with N points it is given by:

$$\Delta r_{\text{nom}} = \text{FOV}/N \quad (1.1)$$

For the mathematical description, it is advantageous to define a variable k which describes the gradient strength integrated over time [21]:

$$k(t) = \frac{\gamma}{2\pi} \int_{t-\tau_G}^t G(t') dt' \quad (1.2)$$

with τ_G the duration of the gradient pulse. The variable k can be interpreted as the *spatial*

frequency: the higher the value of k , the faster the spatial variation of the phase of the transverse magnetization after the gradient pulse. The required increment Δk between two successive gradient steps is determined directly by the *FOV*:

$$\Delta k = \frac{1}{FOV} \quad (1.3)$$

The gradient steps are usually applied in increasing order, beginning at $-N \Delta k/2$ and ending at $(N/2-1)\Delta k$. It is, however, advantageous to use gradient values that are distributed symmetrically about zero, from $-(N-1)\Delta k/2$ to $(N-1)\Delta k/2$ [22–24]. Using such a phase encoding scheme yields a purely real pointspread function (cf. section 1.4). The strength of the n^{th} gradient pulse then is:

$$k_n = \left(n - \frac{N-1}{2} \right) \Delta k, \quad n = 0, \dots, N-1 \quad (1.4)$$

For high N , large values of the spatial frequency k are reached, and a small nominal resolution Δr is obtained. If $\rho(r)$ is the signal emanating from location r , the signal that is detected after the n^{th} phase encoding gradient can be written as the integral over the entire object, modulated by a phase which depends on the position and the gradient strength:

$$s(k_n) \propto \int \rho(r) e^{-i2\pi k_n r} dr \quad (1.5)$$

Performing a discrete Fourier transformation on the N acquired signals, one obtains for the signal from the point $n' \Delta r$ (as long as the sampling theorem has been respected and the signal has not been truncated):

$$S(n' \Delta r) \propto \rho(n' \Delta r) e^{i\pi n'(1-1/N)}, \quad n' = -N/2, \dots, N/2-1 \quad (1.6)$$

Except for the phase factor, the image represents the actual distribution of the magnetization in the sample. The phase factor can be compensated by either taking the magnitude of the image, or by applying an appropriate phase correction. Spectroscopic imaging has the considerable advantage that in only one experiment, the spectra from all N voxels are obtained simultaneously. Furthermore, the localization is not affected by chemical shift artifacts.

A disadvantage of conventional spectroscopic imaging is the long minimal duration of an experiment: in contrast to techniques like STEAM or PRESS, which can acquire the spectrum of a voxel in a single transient, spectroscopic imaging requires at least N repetitions. Several methods for fast spectroscopic imaging have been proposed, which sample the signal in the presence of gradients and reduce the minimal duration drastically [25–30]. However, they require high experimental complexity, and do not offer any gain in sensitivity.

1.4 The Spatial Response Function

In contrast to conventional ^1H -imaging or to multi-dimensional spectroscopy techniques, the number N of voxels (i.e. phase encode steps) in spectroscopic imaging is usually very small. This is due to restrictions on the duration and to the low sensitivity of the experiment. The high spatial frequencies of the sample are then inevitably truncated, and the assumptions behind eqn. (1.6) are no longer valid.

A spectroscopic image thus does not reflect the actual distribution of the spins, but its convolution with a function that is caused by the lack of the high spatial frequencies, the *pointspread function PSF* [31–35]. The signal from some location in the sample is found not in only one pixel of the spectroscopic image, but spread out across all pixels. The PSF describes the amplitude of the propagation of the signal from the point r_0 in the sample to the image pixel with coordinate $r_n = n \Delta r$:

$$PSF(r_n, r_0) = \frac{\sin(\pi(r_n - r_0)/\Delta r)}{N \cdot \sin\left(\frac{\pi(r_n - r_0)}{N\Delta r}\right)} \quad (1.7)$$

This equation can be read in two ways: for a fixed r_0 , the *PSF* indicates how the signal from spins at this position is distributed over all pixels of the image. The PSF is a discrete function consisting of N points. A complementary way of interpreting eqn. (1.7) is usually more relevant for localized spectroscopy: for a fixed r_n , its dependence on r_0 yields the spatial response function *SRF*. This continuous function describes the contribution of every point of the sample to the spectrum in one image pixel.

In Fig. 1.3, the shape of the *SRF* for the case of $N = 8$ phase encoding steps obtained with an unfiltered Fourier transformation is shown. Several important properties of Fourier imaging become visible: Not only does the magnetization from inside the volume of interest (*VOI*), nominally placed in the region $n' \Delta r$, contribute to the signal of its image pixel, but a more or less strong *contamination* by signals from outside this pixel is possible. The spatial response function even extends beyond the actual *FOV*. This has to be taken into account for samples that are larger than the *FOV*, and this can cause contamination of voxels close to the edge of the image by signals emanating from the opposite side of the image.

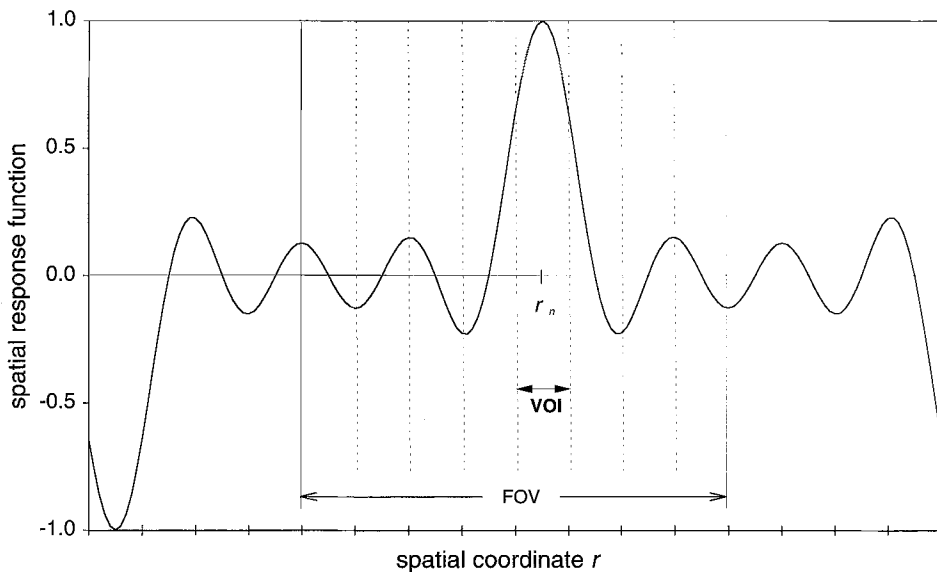


Fig. 1.3: The spatial response function (*SRF*) of a spectroscopic image with $N = 8$ phase encode steps for an unfiltered Fourier transformation. The largest contribution to the signal emanates from the region marked 'VOI'. The *SRF*, however, extends beyond the *VOI* and even beyond the entire *FOV*. Signals from outside the *FOV* thus are aliased into the *FOV*. Mainly signals from sharply edged regions with high signal amplitudes can propagate over the entire image.

The contamination due to the *SRF* is particularly high if regions with a high signal amplitude and sharp edges are present. This situation is given for instance in spectroscopic ^1H -imaging of the brain, where a thin layer of fat outside the skull often contaminates all the spectra in the brain. The quality of the spectra then does not allow reliable

conclusions about the spatial distribution of the examined substances as long as no additional measures are applied to correct or to avoid these effects. Only with an accurate knowledge of the *SRF*, the reliability of an experiment can be assessed.

1.5 Position of a Point Source

In section 1.2, one possible definition for “spatial resolution” was given as the precision in the determination of the location of a single signal source. In the following section, it will be demonstrated that in a Fourier imaging experiment the exact location of a *point source* can be determined with very high precision. The accuracy of this measurement is only limited by the signal-to-noise ratio, and it is in all practical circumstances much better than the nominal resolution. These statements will be further clarified and quantified.

In a one-dimensional situation (see Fig. 1.4), a single point source is located at position x_0 . One conducts N phase-encoded experiments, in each of which the strength of the phase-encoding gradient is incremented by Δk_x . According to eqn. (1.5), the detected signals s_n can be written as:

$$s_n = A e^{-in\Delta k_x x_0}, \quad n = -\frac{N}{2}, -\frac{N}{2} + 1, \dots, \frac{N}{2} - 1 \quad (1.8)$$

In this equation, A is the amplitude of all the signals, and $i = \sqrt{-1}$. The phase φ_n of the measured signals is given by:

$$\varphi_n = \arctan \frac{\text{Im}\{s_n\}}{\text{Re}\{s_n\}} \quad (1.9)$$

From the exponent in eqn. (1.8), one can also recognize the following relation for the phase of the signal:

$$\varphi_n = n \Delta k_x x_0 \quad (1.10)$$

This is the expression of a straight line through the origin, with the slope $m = \Delta k_x x_0$ (cf. Fig. 1.4). If one determines m from the measured values φ_n , the location of the signal

source can be calculated as:

$$x_0 = \frac{m}{\Delta k_x} \quad (1.11)$$

The values of the employed phase-encoding gradients are known, the precision of the calculated position x_0 hence depends mainly from on accuracy of the phase measurement. In principle, it is even possible to determine the position with only two independent experiments.

In Fourier imaging, the detected signals are generally reconstructed with a Fourier transformation. A spatial Fourier transformation can be looked at as a correlation of the measured signal with the reference function $e^{-i\Delta k_x n}$. Through variation of x the frequency of the reference function is changed, and the correlation yields the image of the spatial distribution of the spin magnetization. In our particular case of a single point source, this corresponds to determining the spatial frequency Δk_x in the measured signal. Under these circumstances, (continuous) Fourier transformation and the determination of the slope (eqn. 1.10) are equivalent.

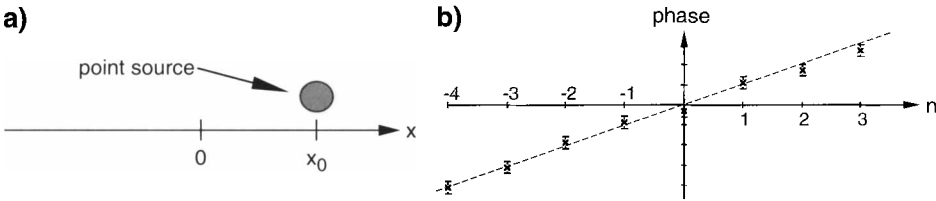


Fig. 1.4: The position of a single point source can be measured with an accuracy that is only limited by the signal-to-noise ratio. a) Let the location of the point source in a one-dimensional setup be x_0 . b) The phase of the NMR signal is measured in $N = 8$ phase-encoded experiments. The location of the point source can be determined from the slope of the obtained phase ramp.

How precisely can one determine the position of a point source, if each of the measured signals is deteriorated by thermal noise? Let the signal-to-noise ratio SNR of each measurement be

$$SNR = \frac{A}{\sigma_s} \quad (1.12)$$

with σ_s being the standard deviation of the thermal noise, and A the signal amplitude in each measurement. The noise in the real and imaginary parts of the signal is independent. How does this noise propagate when computing the phase of the signals? In conventional error analysis, the standard deviation σ_{tot} of a variable $y_i = f(x_1, x_2, \dots, x_i)$ is given by the standard deviations σ_i as:

$$\sigma_{\text{tot}} = \sqrt{\sum_i \left(\frac{\partial f}{\partial x_i} \right)^2 \sigma_i^2} \quad (1.13)$$

In eqn. (1.9), both the numerator and the denominator contain an uncertainty due to the (uncorrelated) noise. Partial derivatives according to eqn. (1.13) yield for the standard deviation of the phase σ_ϕ :

$$\begin{aligned} \sigma_\phi &= \frac{\sigma_s}{1 + \frac{\text{Im}^2\{s_n\}}{\text{Re}^2\{s_n\}}} \sqrt{\frac{1}{\text{Re}^2\{s_n\}} \left(1 + \frac{\text{Im}^2\{s_n\}}{\text{Re}^2\{s_n\}} \right)} \\ &= \frac{\sigma_s}{\sqrt{\text{Re}^2\{s_n\} + \text{Im}^2\{s_n\}}} \\ &= \frac{\sigma_s}{A} = \frac{1}{\text{SNR}} \end{aligned} \quad (1.14)$$

The slope m of the regression line through all phase values is calculated as [36]:

$$\begin{aligned} m &= \frac{N \left(\sum_{n=1}^N n \varphi_n \right) - \sum_{n=1}^N n \cdot \sum_{n=1}^N \varphi_n}{N \sum_{n=1}^N n^2 - \left(\sum_{n=1}^N n \right)^2} \\ &= \frac{12 \left(\sum_{n=1}^N n \varphi_n \right) - 6(N+1) \sum_{n=1}^N \varphi_n}{N^3} \end{aligned} \quad (1.15)$$

The standard deviation σ_m of this slope becomes, using eqn. (1.14):

$$\begin{aligned}
\sigma_m &= \sqrt{\frac{N \sigma_\phi^2}{N^4/12}} \\
&= \frac{\sigma_s}{A} \sqrt{\frac{12}{N^3}}
\end{aligned} \tag{1.16}$$

The position of the point source is calculated from eqn. (1.11). The standard deviation σ_x in this calculation, which is the uncertainty of the position, is related to the standard deviation of the slope as:

$$\begin{aligned}
\sigma_x &= \frac{\sigma_m}{\Delta k_x} \\
&= \frac{\sigma_s}{A} \frac{\sqrt{12}}{\Delta k_x \sqrt{N^3}} \\
&= \frac{1}{SNR} \frac{FOV \sqrt{12}}{N \sqrt{N}}
\end{aligned} \tag{1.17}$$

Incorporating the expression for the nominal resolution $\Delta x = FOV/N$, one finally obtains the following, simple expression for the relative error of the position:

$$\frac{\sigma_x}{\Delta x} = \frac{\sqrt{12}}{SNR \sqrt{N}} \tag{1.18}$$

The error in the determination of the position of a point source is inversely proportional to the signal-to-noise ratio of the individual measurements, and to the square root of the number of phase-encoding steps. With an SNR of 25 and $N = 8$ phase-encoding steps, one obtains $\sigma_x/\Delta x = 0.049$: the precision is more than twenty times higher than the nominal resolution! On the other hand, a low SNR can be the factor limiting the resolution.